16th Australasian Fluid Mechanics Conference
Crown Plaza, Gold Coast, Australia
2-7 December 2007

Liquid Film Falling on Horizontal Circular Cylinders

F. Jafar, G. Thorpe and O.F. Turan

School of Architectural, Civil and Mechanical Engineering
Victoria University (F113), PO Box 14428, Melbourne
Australia 8001

Abstract

The objective of this study is to investigate experimentally and numerically the behaviour of liquid film flow over horizontal cylinders. Numerical simulations are performed using a CFD code (FLUENT) for 2D configurations with one, two and three cylinders. The numerical results have been compared with the present experimental results as well as those from the literature. The flow modes and film thickness are reported for the Reynolds numbers range of 400 and 3200. The effect of cylinder separation on the film flow is investigated.

List of Symbols

Ar   Archimedes number $= g \, \rho^2 \, D^3 / \mu^2$

D   Tube diameter, m

g   acceleration due to gravity, m/s^{-2}

Ga   Galileo number $= \rho \, \sigma^3 / \mu^4 g$ (dimensionless)

Re   Film Reynolds number $= 4\Gamma / \mu$

S   Distance between tubes, m

Greek symbols

ρ Density, $= 998.2$ kg/m^3 for water

μ Newtonian dynamic viscosity, kg/m.s
        $= 0.001$ kg/m.s for water

σ Surface tension, kg/s^2
        $= 0.073$ for water

Γ Mass flow rate of the liquid film per unit length of tube (for each side), kg/ms

δ Liquid film thickness, m

ξ Capillary constant $= [\sigma / (\rho \, g)]^{0.5}$, m

λ Instability wavelength, spacing between neighbouring jet or droplets, m

1. Introduction

Liquid films flows over horizontal tubes are encountered in several industrial processes such as in chemical petroleum refining, and heat exchangers. These flows are significant in desalination, refrigeration and food and dairy industries.

This paper is a progress report of the present study towards effective cooling of fresh horticultural produce. It contains experimental and 2D numerical predictions compared with those obtained from the literature.

In 1936, Adams and Conn [1] studied falling liquid film in heat exchangers. They reported advantages where the pressure drop of the liquid flowing over tubes is negligible, the quantity of cooling liquid required was small and the heat transfer coefficients were high. Maron – Moalem et al [2] experimentally observed several working media of falling film liquid over a tube. These researchers focused on dripping characteristic and not on mode transitions. In 1980, Yung et al. [3] studied the flow mode transitions, they associated the mass flow rate for a transition

from the droplet mode to the jet mode with the capillary effect of through the capillary constant, ξ. The flow rate per unit length of the tube at the transition was given by

$$\Gamma = 0.81 \, \frac{\sigma}{\lambda} \, \frac{\pi dp^3}{6} \, (\frac{2\pi\sigma}{\rho\lambda^3})^{\frac{1}{2}} \qquad (1)$$

where

$$\lambda = \xi \, [4 \, \pi^2 \, n]^{0.5} \qquad (2)$$

n = 2 and d_p is the diameter of primary drops, experimentally determined for water and alcohol to be

$$d_p = 3 \, \xi \qquad (3)$$

Rogers [4] solved the motion and energy equations for laminar film flow falling on horizontal tubes. He calculated the laminar film thickness at any position as function of Reynolds number (Re), Archimedes number (Ar) and the angular position on the horizontal tube.

Mitrovic [5] investigated the falling film - flow mode-transitions of adiabatic and non–phase change film for plain tubes and found that transition from the droplet mode to the jet mode occurred at Reynolds numbers between about 150 and 200. The transition from jet mode to the sheet mode occurred at Reynolds numbers between 315 and 600. He also found that the heat transfer coefficient increased with feeder height, along the whole surface perimeter. The falling-film mode-transitions from Mitrovic are shown in Figure 1.

Honda et al. [6] presented several transition expressions for fluids condensing on low finned tubes, their study are similar to that of an adiabatic falling film of Mitrovic [5].

Rogers and Goindi [7] experimentally calculated the film thickness of water falling on a circular horizontal tube as follows:

$$(\frac{\delta}{d})_{min} = 1.186 \, \mathrm{Re}^{\frac{1}{3}} \, Ar^{-\frac{1}{3}} \qquad (4)$$

Armbruster and Mitrovic [8] modelled the mode transitions for droplet, jet and sheet modes according to

$$\mathrm{Re} = A \, \mathrm{Ga}^{\frac{1}{4}} \qquad (5)$$

where A is an empirical constant whose value defines the type of transition. They observed the mode transition depended on the liquid mass flow rate, only, regardless of increasing or decreasing mass flow rates.

Fujita and Tsutsui [9] defined the two flow modes as follows:

1. Separate droplet mode, characterized by the liquid falling as jet and then, separated into droplets as the falling velocity increases

2. Jets mode, characterized by the collapse of neighbour jets, resulting in a sheet, followed by its separation.

They have recorded that the transition between the droplet and the second mode occurred at Reynolds number around 100, which is agrees with Mitrovic [5].

Hu and Jacobi [10, 11] studied the falling-film flow-mode transitions under adiabatic conditions for a variety of fluids, tube diameters, tube pitches and flow rates as it shows in Figure 2. They proposed that the flow-mode transition map coordinated with film Reynolds number (Re) and the Galileo number (Ga). The map shows transition among the three dominant modes (droplet, column and sheet) with two mixed mode zones (droplet – column and column – sheet). The corresponding four flow transitions among these five zones are given below for plain tubes and air velocity under 15 m/s. The transitions is in either direction, as denoted by a double-headed arrow, $\leftrightarrow$:

Droplet $\leftrightarrow$ Droplet – Column: $\text{Re} = 0.074\,\text{Ga}^{0.302}$ (6)

Droplet – Column $\leftrightarrow$ Column: $\text{Re} = 0.096\,\text{Ga}^{0.301}$ (7)

Column $\leftrightarrow$ Column – Sheet: $\text{Re} = 1.414\,\text{Ga}^{0.233}$ (8)

Column – Sheet $\leftrightarrow$ Sheet: $\text{Re} = 1.448\,\text{Ga}^{0.236}$ (9)

The Galileo number of the liquid is defined as

$$\text{Ga} = \frac{\rho\ \sigma^3}{\mu^4\,g}$$ (10)

and the liquid film Reynolds number is defined as

$$\text{Re} = \frac{2\Gamma}{\mu}$$ (11)

where Γ is the total mass flow rate on both sides of the tube. μ is the liquid dynamic viscosity, and σ is the surface tension, $\sigma = 0.073$ N/m obtained from Roques et al [12], ρ is the density and g is the acceleration due the gravity.

Roques et al [12] presented inter-tube flow-mode transition maps for arrays of four plain tubes to observe all three modes (droplet, column and sheet mode). Ouldhadda et al [13] investigated numerically the laminar flow and heat transfer in non–Newtonian falling liquid film on a horizontal cylinder for constant heat flux and isothermal boundary conditions. They studied water film thickness with different mass flow rates and found that the effect of mass flow rate on the enhancement of the heat transfer coefficients was small.

Mohamed [14] investigated the flow behaviour of liquid falling-film on horizontal stationary and rotating tubes. He investigated the transition modes and column departure wavelengths. He concluded that when liquid film fell on a horizontal rotating tube, the transition from one mode to the next started at a lower Reynolds number than for a stationary tube. Also, rotation was more effective on transition from droplet mode, at a lower Reynolds number, than it was from jet mode. The lowest effect of rotation was for the sheet mode when the Reynolds number was the highest.

The two-dimensional half-domain shown in Figure 3, was modelled numerically in the present study. Following a

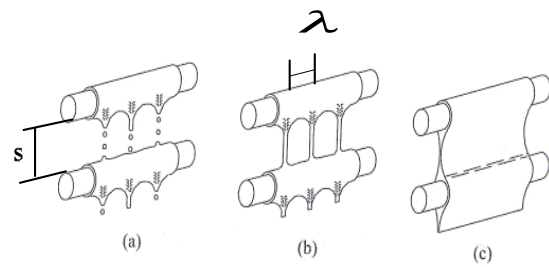description next of the present experimental setup, the numerical model is described,

Figure 1. The idealized intertube of falling film modes; (a) droplet mode, (b) jet mode, (c) the sheet model. Mitrovic [5].
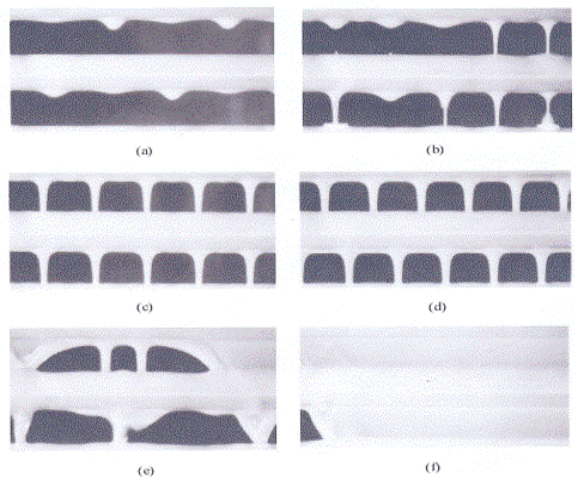

Figure 2. The observed falling film modes reported by Hu and Jacobi [10, 11]: (a) droplet; (b) droplet-jet; (c) inline jet; (d) staggered jet (c) jet -sheet; (f) sheet mode.
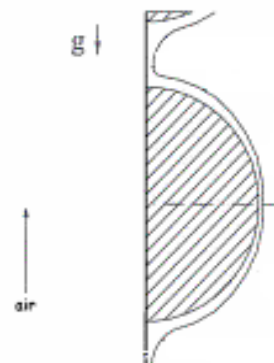

Figure 3. Half domain. The mass flow rate of liquid film has been taken for one side, only.

2

2. Experimental setup

A photograph and a sketch of the experimental setup are shown in Figures 4 and 5, respectively. The apparatus is made up of four parts, a water tank, three cylinders, a cylinder rack, and a collection tub. The cylinder rack enables the vertical separation adjustment of the cylinders. It is possible to observe just one cylinder, or two cylinders or three, with this arrangement.

The cylinder dimensions are, 0.1-m diameter and 0.3-m length. There is a slot of 0.003-m width at the base of the water tank to allow a thin sheet of water to be released towards the first cylinder. The slot width is also adjustable.

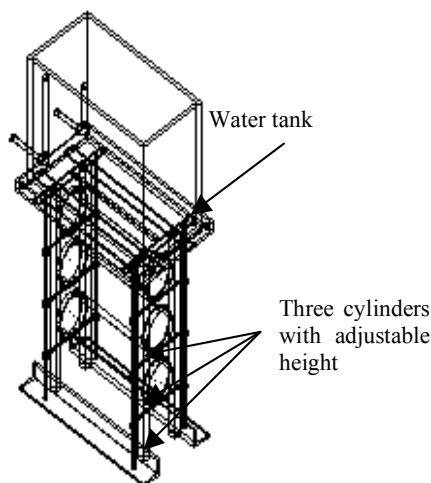Figure 4. A photograph of the apparatus

Figure 5. Sketch of the experimental setup

3. Numerical model

3.1 Grid generation

Numerical simulations have been performed for different mass flow rates to track the water flow falling over one, two and three cylinders. A commercial finite volume CFD code, FLUENT has been used. 2D simulations have been implemented with similar characteristics of mesh generation, solver setup and laminar flow conditions for 0.1 and 0.2 kg/ms mass flow rate and a turbulent flow model (kω) for 0.4, 0.6 and 0.8 kg/ms.

In Figure 6, the numerical model of one cylinder is illustrated. As mentioned in relation to Figure 3, half of the domain has been modelled in order to obtain faster solution. The top right boundary of 0.0015 m represents the velocity inlet, where different velocities of 0.066, 0.133, 0.27, 0.4 and 0.53 m/s are employed to achieve different mass flow rates of 0.1, 0.2, 0.4, 0.6 and 0.8 kg/ms. The top left boundary represent the pressure inlet. The left vertical boundary represents the pressure outlet, and the right side the symmetry boundary. The bottom boundary is the pressure outlet, and the radius of 0.05 m represents the cylinder's wall. The same approach has been employed to model two and three cylinders as shown in Figure 7.

Tri-Pave mesh has been generated for the domain of one, two and three cylinders. The areas around the cylinder wall have been carefully meshed by using a boundary layer technique to observe the water flow around the cylinder and to precisely calculate the water film thickness. The thickness of the first boundary layer around the cylinder is 0.00015 m with a growth factor of 1 and for 20 rows. A size function technique has been employed with a growth factor of 1.1, with starting size of 0.001 m with a size limit of 1. . This technique helps to refine and minimise the grid size where needed and maximise where relatively small gradients are expected.
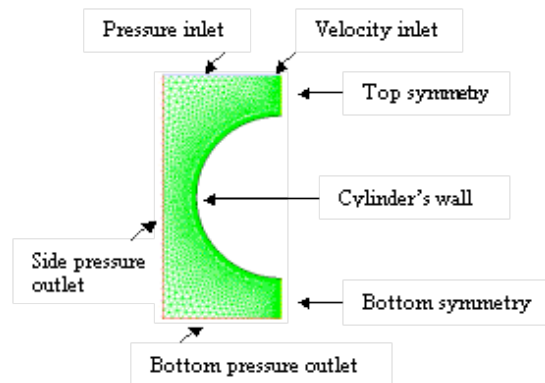
Figure 6. Half-domain numerical model with the boundary conditions.

The grid has been generated in Gambit. In Table 1, the 2D simulation settings in FLUENT are listed.

Settings	Choice
Simulation	2D
Solver	Segregated implicit
Model	VOF
Material	Air – primary and water – secondary
Gravitational acceleration	-9.81
Volume fraction	1 for water and 0 for air
Pressure Velocity Coupling	PISO
Discretization Pressure	PRESTO
Discretization Momentum	1 Order Upwind
Top boundary	Velocity inlet and pressure inlet
Left side boundary	Pressure outlet
Right side boundaries	Symmetry
Bottom side boundary	Pressure outlet
Wall boundary	Cylinder's edge

Table 1. FLUENT 2D simulation settings

The objective of the first series of simulations was to study the falling-water film-thickness over one cylinder for different mass flow rates of 0.1, 0.2, 0.4, 0.6 and 0.8 kg/ms to compare with the literature. Subsequently, with 2D numerical models of two and three cylinders, the effect of cylinder separation on film flow has been studied.
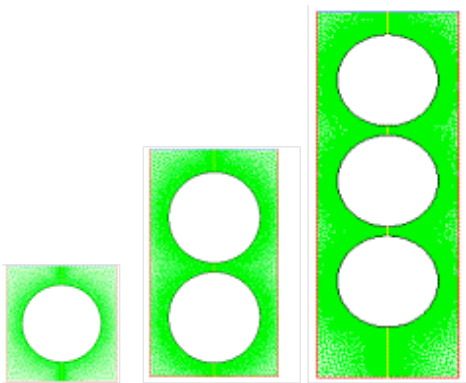
3.2 Grid independence

To study grid independence, three simulations have been done with a constant mass flow rate of 0.4 kg/ms using 4708, 7060 and 10201 total grid elements. In Figure 8, it is shown that the numerical results of water film thickness, as a function of the azimuthal position around the cylinder, with the coarsest of these three grids, are grid independent
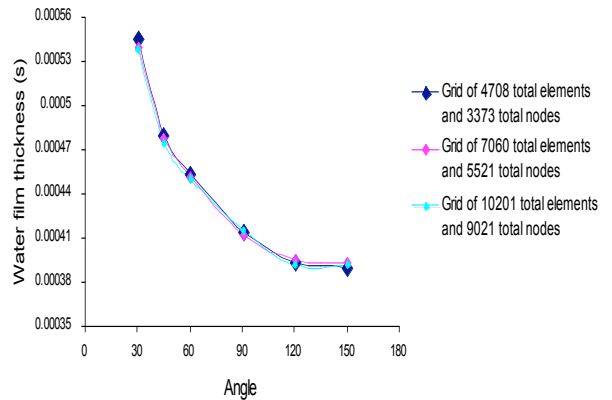
Figure 8. Grid independence

3.3 Time-step independence

To check time-step independence, 4708 total grid elements were used with a mass flow rate of 0.4 kg/ms. The simulations were run for three time steps of 0.0025 s, 0.00125 s and 0.000625 s. In Figure 9, it is shown that the results are time-step independent with the largest of these time steps.
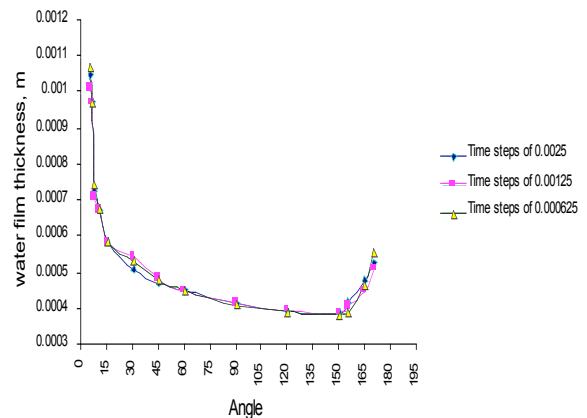
Figure 7. Grid used for one, two and three cylinders after mirroring half domains.

Figure 9. Time-step independence.

4

1196

4. Results and discussion

4.1 Experimental results of falling film mode

Sets of experiments are conducted using water as the test fluid, and at mass flow rates of 0.1 and 0.2 kg/ms. It is found that the falling-liquid film modes are the jet–sheet and sheet modes, respectively. In Figures 10 and 11, these flow modes are illustrated for Reynolds numbers of 400 and 800, respectively. A high speed CASIO digital video camera was used to record and observe the phenomena in slow motion to facilitate detection of the modes. These experimental results are in agreement with the results of Armbruster and Mitrovic [8].
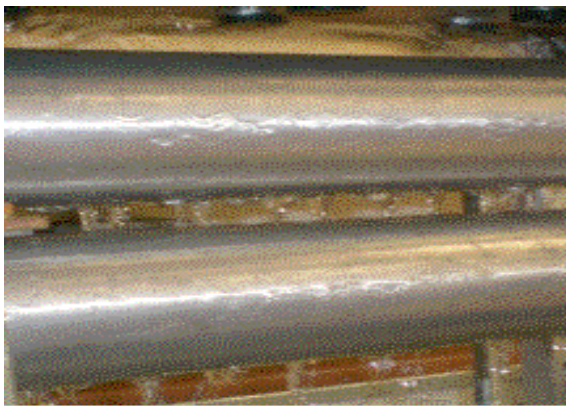

Figure 10. The flow pattern for Re = 400 (corresponding to a mass flow rate of 0.1 kg/ms. The jet-sheet (continuous column) mode is observed.
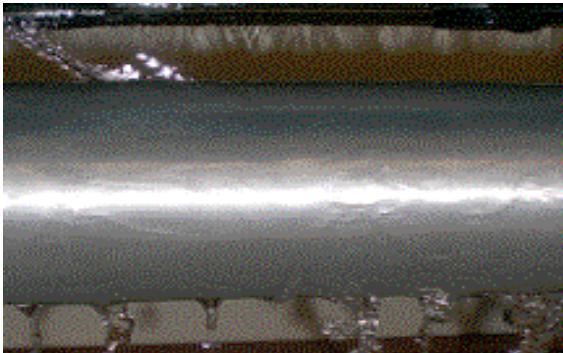

Figure 11. The flow pattern for Re = 800 (0.2 kg/ms). The sheet mode is present between the two cylinders.

It has been observed that the transition depends on the liquid mass flow rate. The droplet mode starts at low Reynolds numbers. As low as Re = 150 was observed here. As the flow rate increases, a jet mode followed by the collapse of neighbouring jets, leads to a sheet mode. In Figure 12, a comparison is given between the current experimental results and those of Armbruster and Mitrovic [8].

In Figure 10, the wavelength λ is approximately equal to 0.024 m, in agreement with Equation (2).
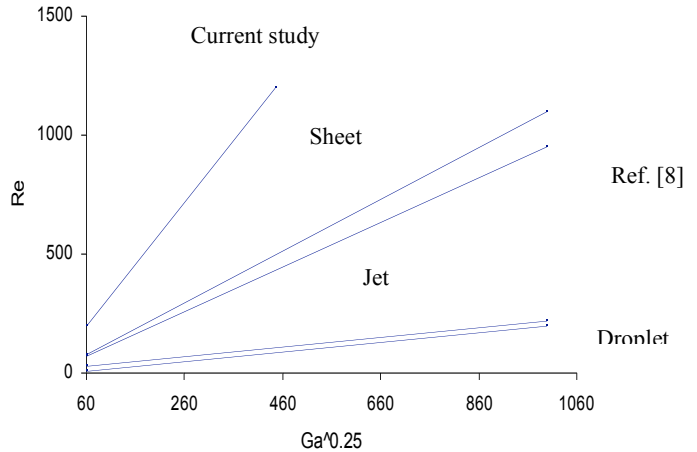

Figure 12. Comparison of correlations for flow mode transitions between the current study and Armbruster and Mitrovic [8].

4.2 Water film thickness δ

In this study, Archimedes number has been calculated to be 10^{10} and water film thickness has been calculated from Equation (4) to be 0.000823m. The water film thickness from the current numerical simulations is 0.0008 m (at 90° from the vertical, at Re = 1600), in close agreement.

4.3 Further comparisons

The 2D simulations of water film-flow over cylinders have been carried out for velocities of 0.066, 0.133, 0.27, 0.4 and 0.53 m/s to achieve 0.1, 0.2, 0.4, 0.6 and 0.8 kg/ms of mass flow rates, respectively. The simulations are multiphase, where air is treated as a primary phase and water as a secondary phase.

The water film thickness has been calculated at different positions around the perimeter of the cylinder for different mass flow rates. The thickness is the largest at the top and bottom of the cylinder, and narrowest at either side. The water film thickness is less for a lower mass flow rate and greater for a larger mass flow rate, in agreement with Ouldhadda et al. [13] In Figure 13, the variations of film thickness is shown over the tube for different mass flow rates. From the numerical results, the correlation between film thickness and the mass flow rate was also studied.
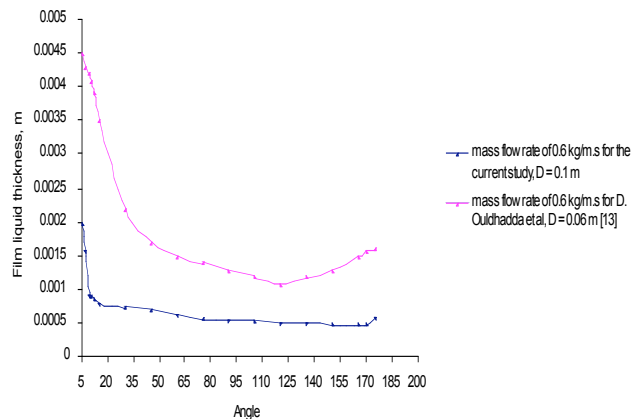

Figure 13. Comparison between the current study and Ouldhadad et al. [13].

4.4 Numerical results of liquid film flow over one, two and three cylinders

Simulations have been performed with one cylinder to study the water film thickness and to compare the results with the literature, as described in Section 4.3 above. Subsequently, film flow over two and three cylinders was studied

In Figure 14, the water flow starts from the top at the inlet boundary, and it goes around the circumference of the tube, down to the outlet boundary.
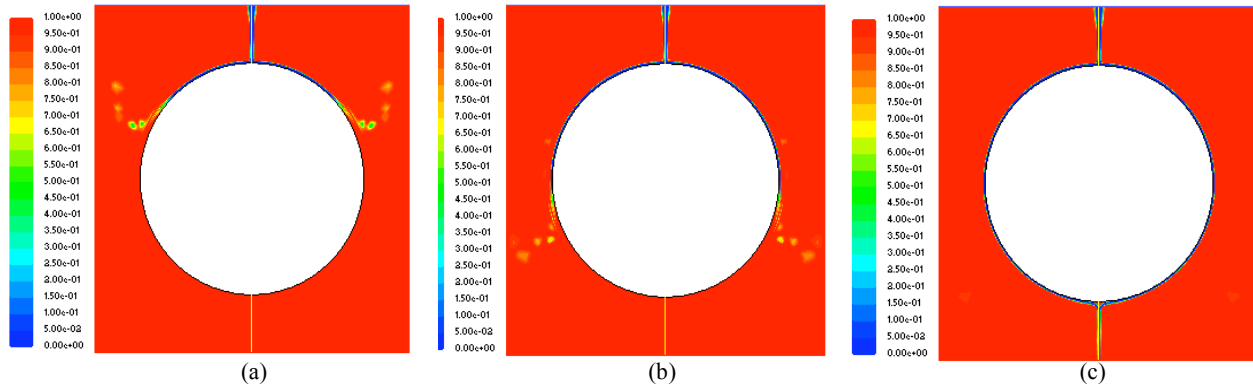

Figure 14. Falling liquid over the cylinder at different time where the air phase in red and water in blue, (a) the liquid film at the top of the cylinder; (b) at the centre of the cylinder; (c) the liquid film is complete around the cylinder.

In Figure 15, the water film flows is over two cylinders. The distance between the two tubes is, 0.02 m. The Reynolds number for this simulation is 400. The mode of the falling water between the two cylinders is a column sheet, in agreement with Armbruster, and Mitrovic [8].
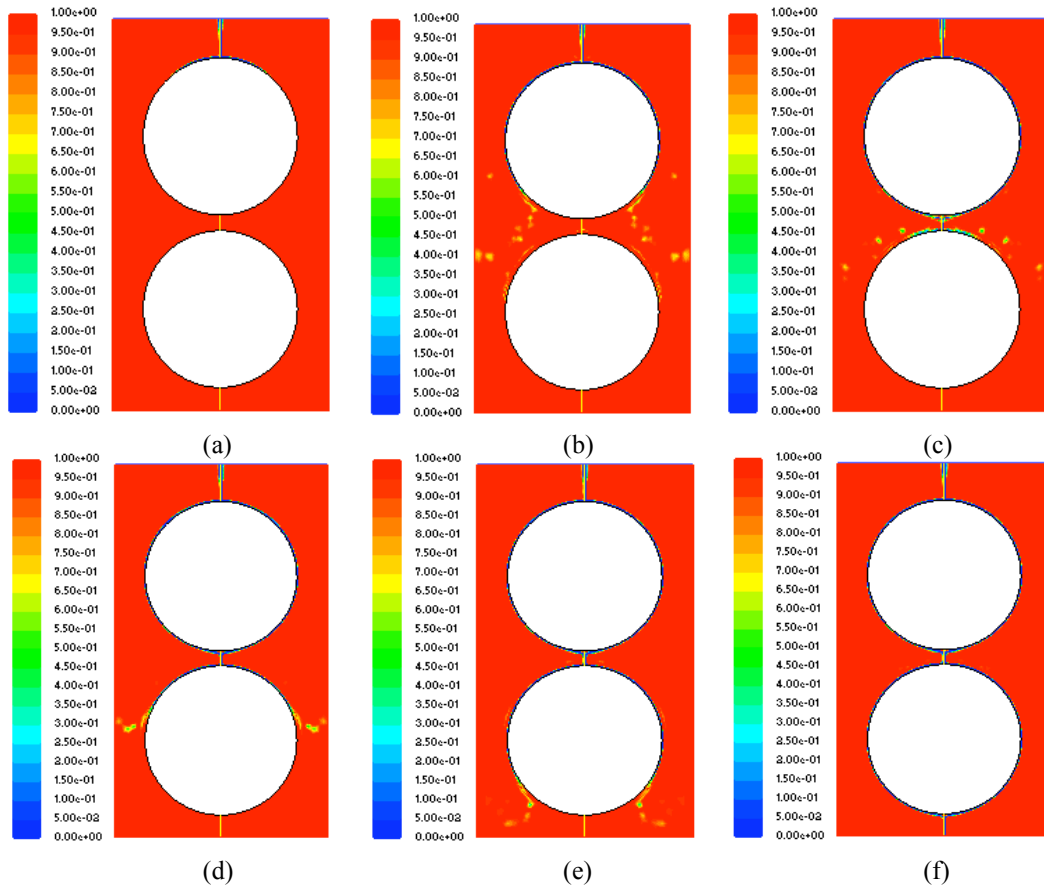

Figure 15. Falling film over two cylinders at different times (a) The liquid film over the top of the first cylinder; (b) at the bottom half of the first cylinder; (c) at the separation part between the two cylinders; (d) at the top half of the second cylinder; (e) at the bottom half of the second cylinder; (f) completion of the falling liquid film over the two cylinders

6

In Figure 16, the simulation of falling film is shown when three cylinders instead of two are present, using the same separation distance of 0.02 m and the same Reynolds number. The results show that the mode of the falling film between the first tube and the second is the same as that between the second and the third.
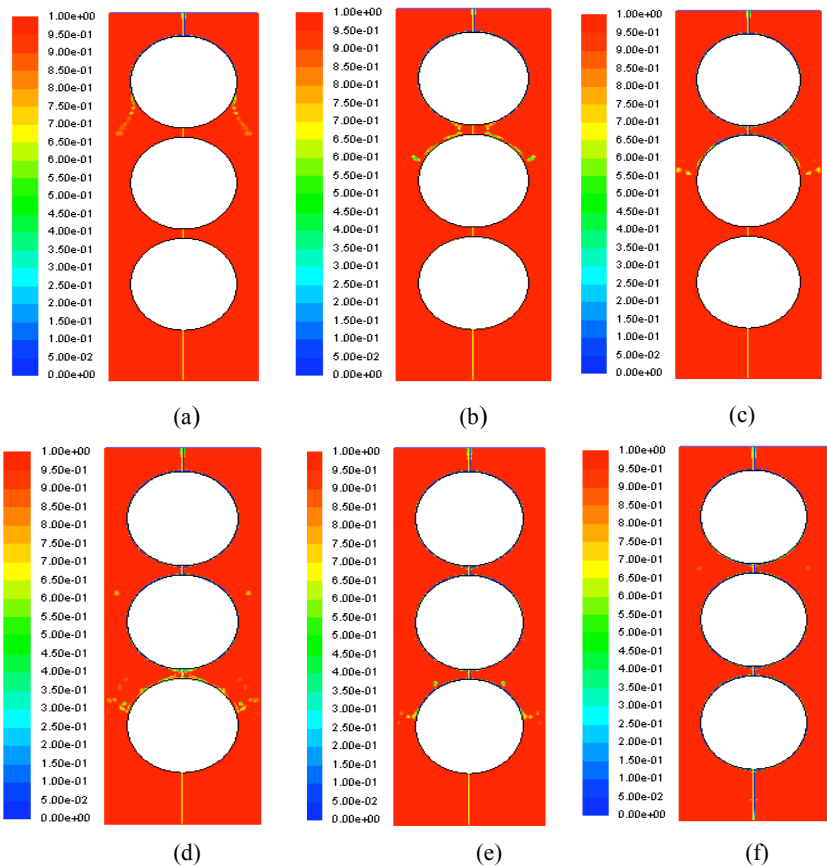

(a)   (b)   (c)

(d)   (e)   (f)

Figure 16. Falling film over 3 cylinders at different times (a) the liquid film at the center of the first cylinder; (b) at the separation part between the first and second cylinder; (c) at the top of the second cylinders; (d) at the separation part between second and third cylinder; (e) at the top of the third cylinder;(f) completed falling film over three cylinders

Another simulation has been performed to study the effect of separation distance by separating two tubes by 0.03 m. In Figure 17, the separation distance is 0.02 m, and the falling film is a sheet.
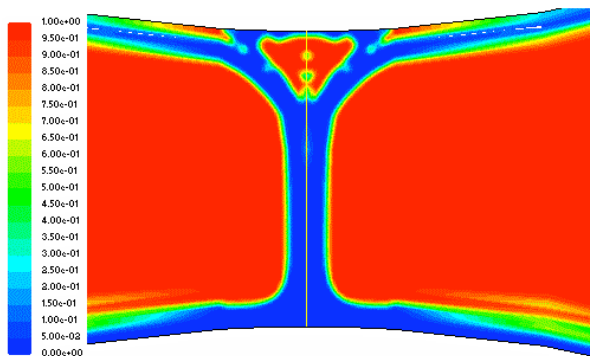
In Figure 18, the separation distance is 0.03 m where the falling film is still a sheet, but the thickness of the liquid film is slightly less than that for the 0.02-m separation.
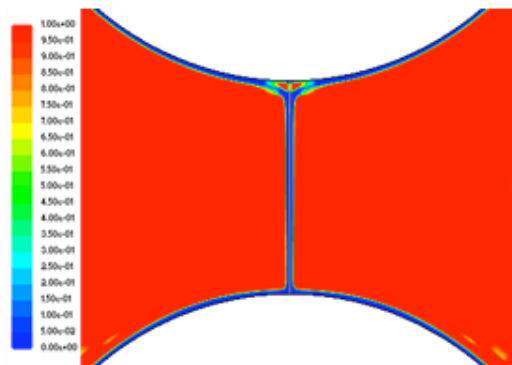

Figure 17. The separation is 0.02 m and the falling film is a sheet mode.

Figure 18. The separation is 0.03 m and the falling film is a sheet mode

7

5. Conclusions

In this paper, a progress report is presented of an experimental and numerical study of liquid-film flowing over horizontal cylinders. The existing literature has been reviewed extensively. The current experimental and numerical results are so far in agreement with the results from the literature. The numerical tool chosen for the present study, FLUENT, has enabled close examination of the flow field. Further work is under way with the addition of heat transfer characteristics along with a 3D geometry towards efficient cooling of horticultural fresh produce.

Acknowledgement

References

1. Adams, F. W. and Conn, A. L. A horizontal film type cooler – film coefficients of heat transmission, Industrial Engineering Chemistry 28, 1936: P 537.
2. Maron – Moalem, D., Sideman, S., and Dukler, A. E., Dripping Characteristics in a Horizontal Tube Film Evaporator. Desalination 27, 1978: P 117 – 127.
3. Yung, D., Lorentz, J. J., and Ganic, E. N., Vapor/Liquid Interaction and Entrainment in Falling Film Evaporators. "ASME Journal of Heat Transfer. 102, 1980: P 20 – 25.
4. Rogers, J. T. Laminar falling film flow and heat transfer characteristics on horizontal tubes, Canadian Journal of Chemical Engineering 59, 1981: p213 – 222.
5. Mitrovie, J., *Influence of Tube Spacing and Flow Rate on Heat Transfer from a Horizontal Tube to a Falling Liquid Film.* Proc. 8th International Heat Transfer Conf. San Francisco. 4, 1986: p. 1949 - 1956.
6. Honda, H., S. Nozu, and Y. Takeda, *Flow Characteristics of Condensation on a Vertical Column of Horizontal Tubes.* ASME - JSME Thermal Engineering Joint Conference, Honolulu. 1, 1987: p. 517 - 524.
7. Rogers, J. T and Goindi, S.S. Experimental laminar falling film heat transfer coefficient on a large diameter horizontal tube, The Canadian Journal of Chemical Engineering 67 1989: p. 560 – 568.
8. Armbruster, R. and Mitrovic. J. Patterns of falling film flow over horizontal smooth tubes. Proceedings of the 10th international heat transfer conference, Brighton. 3 1994: p. 275 – 80.
9. Fujita, Y. and Tsutsui, M. Evaporation heat transfer of falling films on horizontal tube. Part 2. Experimental study Heat Transfer _ Jpn Res 24, 1995: p. 17 – 31.
10. Hu, X. and A.M. Jacobi, *The Intertube Falling Film Part 1 - Flow Characteristics. Mode Transitions and Hysteresis.* ASME J. Heat Transfer. 118, 1996: p. 616 - 625.
11. Hu, X. and A.M. Jacobi, *The Intertube Falling Film Part 2 - Mode Effects on Sensible Heat Transfer to a Falling Liquid Film* ASME J. Heat Transfer 118, 1996: p. 626 - 633.
12. Fujita, Y. and Tsutsui, M. Experimental investigation of falling film evaporation on horizontal tubes. Heat Transfer _ Jpn Res 27 1998: p. 609 – 618.
13. Ouldhadda, D., A.I. Idrissi, and M. Asbik, *Heat transfer in non - Newtonian falling liquid film on a horizontal circular cylinder.* Heat and Mass Transfer. 38, 2002: p. 713 - 721.
14. Roques, J. F, Dupomt, V., and Thome, J. R, *Falling Film Transition on Plain and Enhance Tubes.* J. Heat Transfer. 124, 2002: p. 491-499.
15. Mohamed, A.M.I., *Flow behavior of liquid falling film on a horizontal rotiting tube.* Experimental Thermal and Fluid Science. 31, 2007: p. 325 - 332.

8